



Virtual sensing of load forces in hydraulic actuators using second- and higher-order sliding modes

Michael Ruderman^{a,*}, Leonid Fridman^b, Philipp Pasolli^a

^a Faculty of Engineering and Science, University of Agder, Norway

^b Engineering Faculty, National Autonomous University of Mexico, Mexico



ARTICLE INFO

Keywords:

Robust exact differentiator
High-order sliding mode observer
hydraulic actuator
force sensing

ABSTRACT

External load forces are challenging for sensing or estimating in the hydraulic actuators. Once it is due to inconvenient instrumentation of the force sensors, especially on an open-end mechanical interface. The other way, the complex nonlinear system behavior aggravates reconstructing the system states in a robust and real-time suitable manner. This paper proposes a sensorless estimation of external load forces in standard hydraulic actuators by using a well-established equivalent output injection of the second-order sliding mode and also higher-order sliding mode differentiator. Only the basic inertial and frictional parameters are assumed to be known from an initial identification without external load. Afterwards, the robust exact differentiators are used in order to reconstruct the system states. Noisy signals of the cylinder chamber pressures and piston stroke are the single quantities available from the measurement. An experimental case study, accomplished on the setup of two hydraulic cylinders arranged and operated in antagonistic way, is provided. The force-cell on the rigid interface between both cylinders is used for reference measurements and evaluation of the estimation algorithms. Two estimation approaches, one of the 2nd and another of the 4th order, are assessed in performance and compared to each other along with discussion.

1. Introduction

Hydraulic actuators are generally known to exhibit complex non-linear behavior that is inherent due to forward and feedback couplings of the corresponding electro-magnetic, hydraulic, and mechanic subsystems, see e.g. basic literature (Jelali & Kroll, 2012; Merritt, 1967). While the time response, correspondingly transient dynamics, of hydraulic actuators can be seen as relatively slow, comparing for instance with pneumatic cylinders, electric motors, and linear drives, a linearization of hydraulic systems and order reduction of the whole dynamics yield challenges for analysis and control design. Besides, the large-scale machines actuated by hydraulic cylinders are also known to operate frequently with the heavy payloads and within harsh, to say ‘non-clean’, and predominantly outdoor environments. Throughout almost all of them require at least semi-automatic control, the application examples are numerous like excavators (Ha, Nguyen, Rye, & Durrant-Whyte, 2000; Haga, Hiroshi, & Fujishima, 2001), forestry machines (Mattila, Koivumäki, Caldwell, & Semini, 2017; Ortiz Morales et al., 2014), various-type hydraulic presses (Komsta, van Oijen, & Antoszkiwicz, 2013; Osakada, Mori, Altan, & Groche, 2011), maritime cranes (Küchler, Mahl, Neupert, Schneider, & Sawodny, 2011; Rokseth, Skjong, & Pedersen, 2016), and others. As consequences emanating from the environment like temperature, dust, humidity, wear and varying payloads,

equally as disturbance loads, the hydraulic actuators are generally subject to large uncertainties and perturbations during operation.

In view of the said above, the control and especially robust control of hydraulic actuators have been and yet remain an active research area, see for instance several former works (Bonchis, Corke, Rye, & Ha, 2001; Plummer & Vaughan, 1996; Yao, Bu, Reedy, & Chiu, 2000) and more recent studies (Koch & Reichhartinger, 2016; Pedersen & Andersen, 2018; Won, Kim, & Tomizuka, 2017). Apart from a suitable methodology for the robust control design and decision about underlying control system architecture, it is the limited access to internal system states and unknown load forces (or torques) that poses several challenges on a controlled operation of hydraulic actuators. For instance, a robust estimation (Ruderman & Fridman, 2018; Vázquez, Aranovskiy, Freidovich, & Fridman, 2016) of the piston velocity has to be performed, mostly based the low-resolution and noise-corrupted stroke measurements. Over and above that, a force-controlled operation of hydraulically actuated cylinders generally suffers under unknown load forces, see e.g. in Alleyne and Liu (2000), especially in the endpoint force applications (Lawrence et al., 1997). Several related simulation and experimental studies can be found in the last two decades, see for instance (Jerouane, Sepehri, & Lamnabhi-Lagarrigue, 2004; Loukianov, Rivera, Orlov, & Teraoka, 2009; Taylor & Robertson, 2013) and references therein.

* Corresponding author.

E-mail address: michael.ruderman@uia.no (M. Ruderman).

Among trials to deal with unknown load forces in hydraulic actuators, the sliding mode (SM) (Shtessel, Edwards, Fridman, & Levant, 2014; Utkin, Guldner, & Shi, 2009) based observers belong to efficient methods to estimate the forces as uncertainties (Koch & Reichhartinger, 2016; Komsta et al., 2013; Ruderman & Fridman, 2018; Vázquez et al., 2016). For that aim the Higher-Order Sliding Mode (HOSM) observers, based on HOSM differentiators, can be used. The simplest strategy to estimate the forces suggested in Davila, Fridman, and Poznyak (2006) (see also Komsta et al., 2013) consists of two basic steps: first to apply a super-twisting-algorithm (STA) based observer for estimating state derivative, and then to usage a low-pass filter to reconstruct the forces. An alternative, and theoretically more exact, approach is to use the HOSM differentiators of order two and higher. Note that such higher-order approach is also considered in this work for the sake of comparison. Furthermore, it should be noted that the targeted hydraulic actuators have relatively slow dynamics, with main challenges being rather in disturbances and model uncertainties. Therefore, a single hydraulic actuator is put into focus of this work, while multiple DOF systems, like e.g. hydraulic cranes or excavators, are not explicitly considered. Therefore, the coupling by-effects can be equally attributed to the actuator perturbations.

The main contributions of the recent work, which also differ it from the former results mentioned above, are:

- The STA-based robust exact differentiator (Levant, 1998) is used in cascade with an equivalent output injection technique (Davila et al., 2006). By doing this, a higher- than second-order estimator is not required. Thus the Lipschitz constant of the second time derivative of the measurable output signal yields the single design parameter of the applied differentiator.
- A proposed cascade approach is shown in comparison with a HOSM-based approach, while the third-order differentiator proved to be sufficient for reconstructing both, the relative velocity and acceleration required for an external load force estimation.
- The nonlinear friction modeling, robust against the noisy velocity signals, is incorporated into description of the nominal system dynamics. The modeling approach takes into account most of the transient and steady-state friction effects, it also avoids discontinuities at zero crossing. Avoiding additional discontinuities in the nominal system dynamics at frequent velocity zero crossings appears particularly relevant for the generated sliding-mode. Recall that the sliding-mode self is driven by injecting discontinuities of the estimation error.
- The proposed virtual force sensing is experimentally evaluated on a standard industrial hydraulic cylinder setup with low-accuracy stroke sensing, and that for a large variation of the external load forces.

The rest of the paper is organized as follows. In Section 2, the hydraulic actuator system is introduced and the system modeling including complex nonlinear friction is given. The second-order sliding mode approach together with associated gain tuning and equivalent output injection, including low-pass filtering, are described in Section 3. Following to that, a higher-order sliding mode approach considered for comparison is addressed in Section 4. A comparative experimental evaluation of predicting the reference-measured external load force of different amplitudes and frequencies is given in Section 4. The paper is concluded in Section 5.

2. Hydraulic actuator system

2.1. Experimental setup

The experimental system considered in this study consists of two identical linear hydraulic cylinders arranged in antagonistic way, see laboratory view depicted in Fig. 1. Both cylinders are rigidly coupled to

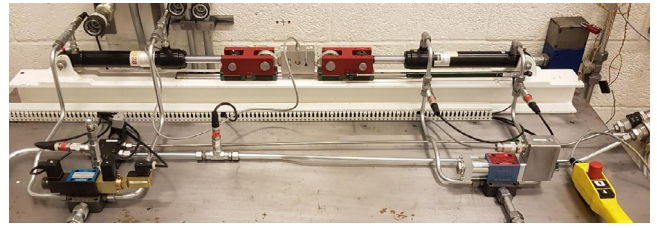


Fig. 1. Experimental setup of hydraulic cylinders.

each other via the force sensor. That allows for reference measurement of the load force imposed on the right-hand side cylinder which is controlled. The right-hand side cylinder is driven via the 4/3 servovalve and constitutes the object of investigation. The left-hand side cylinder is powered via a directional control valve, connected in series with a pressure reduction valve, thus allowing to generate a counteracting load force. The latter is controlled in an open-loop manner. In addition to linear potentiometer, for recording the cylinder stroke, i.e. relative displacement, the pressure sensors are installed for both chambers of cylinder. All input and output signals are provided via the real-time control board with 2 kHz sampling rate. For more details on the experimental setup an interested reader is referred to Pasolli and Ruderman (2018, 2019).

2.2. System dynamics

The dynamics of hydraulic actuator, linear cylinder in the recent case, is assumed to be of the second-order for the given hydraulic force $u = A_r P_r - A_l P_l$. Here the pressures and effective piston areas are denoted by $P_{r/l}$ and $A_{r/l}$ for the right- and left-hand side chambers correspondingly. Since the pressure measurement is available for both chambers, and the piston cross sections are assumed to be accurately known from technical data, the input force $u(t)$ appears as an exogenous system excitation, i.e. system input to be known. For a relative motion with 1-DOF, the system dynamics is given by

$$m\ddot{x} + f(\dot{x}) + F = A(P_r - nP_l). \quad (1)$$

The overall moving mass is aggregated to the lumped inertial parameter m . The relative ratio $0 < n < 1$ captures the difference between the full (effective) cross-section of the piston, on the right-hand side, and its reduced area on the left-hand side. The latter is obviously due to a one-side piston rod. An unbounded relative displacement in x -coordinates is assumed. That means the mechanical bad-stops at the cylinder limits are not explicitly taken into account. The relative motion of the piston rod is counteracted by an external load force $F(t)$ which is generally unknown and, therefore, represents the target of virtual sensing. The total friction force of hydraulic cylinder is denoted by $f(\cdot)$. It is stressed that x is the single measurable output state, in addition affected by the sensor noise, and neither $\dot{x}(t)$ nor $\ddot{x}(t)$ are available from measurements.

2.3. Nonlinear friction

For capturing the frictional behavior, three most relevant effects of the dynamic friction force are taken into account. Note that the dynamic friction force is understood here with one DOF, and that acting in opposite direction to the relative displacement. Apparently, three coupled by-effects of the nonlinear friction are the viscous frictional damping, the so-called Stribeck effect of the velocity weakening curve, see e.g. Armstrong, Dupont, and De Wit (1994), and the continuous presliding transients of the Coulomb friction at motion reversals. Despite the nonlinear friction modeling has attracted considerable attention in the last decades, see e.g. Al-Bender and Swevers (2008), Armstrong et al. (1994) and Marques, Flores, Claro, and Lankarani (2016), the existing empirical and, often, ad-hoc approaches show up various advantages

and disadvantages at the same time. To the large part, they can also be seen as case-varying, correspondingly, case-specific. Especially in terms of a stable and noise-insensitive numerical implementation, also with real-time capability, there are less approaches that found a commonly acknowledged consent. Moreover, a parametric and, correspondingly, identification-related complexity play frequently the most crucial role in a practical friction modeling. The approach formulated below relies on several findings that have been observed experimentally, analyzed, and reported in the previous works (Ruderman, 2017b; Ruderman & Iwasaki, 2015, 2016).

The Stribeck (1902) velocity-weakening curve, cf. Armstrong et al. (1994),

$$S(\dot{x}) = F_c + (F_s - F_c) \exp(-|\dot{x}|^\delta V^{-\delta}), \quad (2)$$

maps the steady-state velocity onto the sign-symmetrical friction force, the magnitude of which decreases exponentially towards the Coulomb friction level $F_c > 0$ during the velocity progresses. The maximal amplitude of the stiction force, that in vicinity to zero velocity, is given by $F_s \geq F_c$. The velocity normalization factor $V > 0$ determines the rate of exponential convergence, while δ is the shaping factor of the velocity-weakening curve. Note that the viscous friction term is not explicitly included in (2) as, otherwise, often done when talking about the static Stribeck-type friction models. Further we notice that (2) does not account for the velocity sign, since the latter will be captured, later on, through the sign-dependent presliding transients, cf. further with (6).

The viscous friction damping, acting on a lubricated contact interface during gross-sliding (roughly speaking continuous motion), can be captured in a standard way by the linear friction coefficient σ . This yields the velocity-proportional term $\sigma \dot{x}(t)$ superimposed to (2).

The discontinuity-free transients of the Coulomb friction force, upon the relative motion reversals, can be captured in different manner, while all having to fulfill the rate-independency and to map the so-called presliding hysteresis loops, see e.g. Al-Bender and Swevers (2008) for detail. One should emphasize that the first well-established approach for presliding transitions may be credited to Dahl (1968). Furthermore, a Maxwell-slip structure, equivalent to the Prandtl-Ishlinskii stop-type hysteresis operators (Ruderman & Rachinskii, 2017), can be used equally as an exponential regression of the presliding stiffness upon the motion reversals (Ruderman & Bertram, 2011). According to the tribological study (Koizumi & Shibazaki, 1984), the area of presliding hysteresis loops increases proportionally to the 2nd power of the so-called presliding distance p . Using the scaling factor s , which relates the after-reversal displacement to the presliding distance

$$p = s \int_{t_r}^t \dot{x} dt, \quad (3)$$

which is defined on the interval $p \in [-1, 1]$, one can describe the frictional curvature in presliding by

$$z_0(p) = p(1 - \ln(p)). \quad (4)$$

For the motion reversal instant t_r and the corresponding motion reversal state $z_r := z(t_r)$, the total (normalized) map of presliding friction transitions is given by

$$z(t) = \left| \text{sign}(\dot{x}) - z_r \right| p(1 - \ln(p)) + z_r. \quad (5)$$

It should be stressed that $z(t)$, according to (5), is defined for $p \in [-1, 1]$ only so that $z(t)$ keeps the constant ± 1 value for $|p| > 1$, and that until the next motion reversal. For more details on the presliding friction map (5) it is referred to Ruderman (2017b).

Following the above developments, the entire friction dynamics can be written as, cf. with Ruderman and Iwasaki (2015),

$$\tau \dot{f}(t) + f(t) = \sigma \dot{x}(t) + S(\dot{x}(t)) z(t) + \alpha z(t), \quad (6)$$

where τ is the time constant capturing the so-called frictional lag (Al-Bender & Swevers, 2008). The α -coefficient is introduced as a necessary

damping factor of presliding transients. Note that this allows for adjustable damping, in addition to the rate-independent damping owing to the presliding hysteresis. One can show that at steady-state, i.e. after vanishing of all transients, the entire friction force reduces to

$$\bar{f}(\dot{x}) = \sigma \dot{x} + S(\dot{x}(t)) \text{sign}(z). \quad (7)$$

Here both the relative velocity and saturated presliding states keep their constant values.

3. Second-order sliding-mode based force estimation

3.1. Robust exact differentiator

For estimating the relative velocity, which is unavailable from direct sensing in hydraulic actuator systems, one can apply the standard robust exact differentiator (Levant, 1998) which is based on the super-twisting algorithm (STA) (Levant, 1993). Provided $x_1 := x$ is the single measurable output, the exact differentiator aims for real-time reconstructing the dynamic state $x_2 = \dot{x}_1$, while $|\dot{x}_2| \leq L$ is subject to unknown, yet bounded, perturbation for some positive constant L . The robust exact differentiator is given by

$$\dot{\hat{x}}_1 = k_1 \Psi(e) \text{sign}(e) + \hat{x}_2, \quad (8)$$

$$\dot{\hat{x}}_2 = k_2 \text{sign}(e), \quad (9)$$

where $e = x_1 - \hat{x}_1$ is the output error. It is worth to recall that the error incorporates both the sensing noise and uncertainties, correspondingly non-modeled perturbations, of the second-order system dynamics. The operator $\Psi(\cdot) = \sqrt{|\cdot|}$ provides a state-varying observation gain, which is inverse-quadratically dependent of the error magnitude. For the appropriately chosen parameters k_1, k_2 , which are positive STA gains cf. with Levant (1998), the robust exact differentiator ensures convergence of the states estimate, i.e. $(x_1 - \hat{x}_1) = (x_2 - \hat{x}_2) = 0$, after the finite-time transients. This is valid for an upper bounded second-order dynamics where $L = \text{const} < \infty$ denotes the finite Lipschitz constant — an either known system property or unknown process parameter to be found.

From above it is obvious that an appropriate gains selection requires the second time derivative of system output to be known. For the system dynamics (1), that means an acceleration quantity which is, however, inherently unavailable from the measurements. Recall that the problem statement requires simultaneously both, estimating the relative velocity and reconstructing the unknown load forces acting on hydraulic cylinder. For an optimal gain setting, calculated as proposed in Ventura and Fridman (2019), one assumes

$$k_1 = 2.028 \sqrt{k_2}, \quad k_2 = 1.1L, \quad (10)$$

that aims for minimizing the fast oscillations amplitude, i.e. amplitude of chattering, in the closed-loop of STA. This optimal gain setting has been recently evaluated with experiments by using another hydraulic system as reported in Ruderman and Fridman (2018). Recall that the k_2 -assignment is standard setting for the highest-order derivative, as proposed in Levant (1998) and later confirmed in Levant (2003), Reichhartinger, Spurgeon, Forstinger, and Wipfler (2017) and Ventura and Fridman (2019), see also Shtessel et al. (2014) for more detail.

While L remains the single design parameter, unavailable in the system description, the proposed approach is in determining it via a numerical optimization based on the recorded experimental data. Solving numerically the minimization problem

$$\min_L \sum_{i=1}^N (\dot{x}_i - \hat{x}_{2,i}(L))^2, \quad (11)$$

of the estimation error results in a locally optimal L . The size of the measured data set is denoted by N , while $\hat{x}_{2,i}$ is the estimated velocity state as function of the variable L . The cumulative squared error is shown in Fig. 2 against the varying L , from which the optimal gain $L = 3.1$ is obtained. The relative velocity (cf. further experimental results in

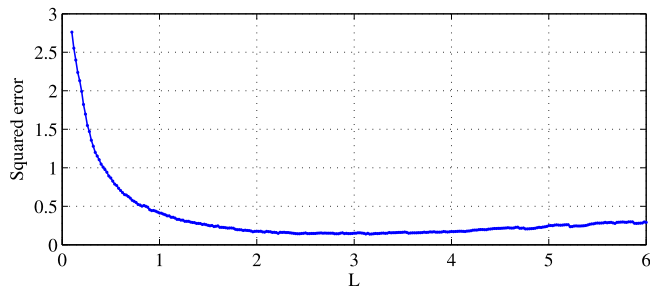


Fig. 2. Cumulative squared error $\sum(\dot{x} - \hat{x}_2)^2$ against L , computed for determining the optimal STA-gain setting according to (10).

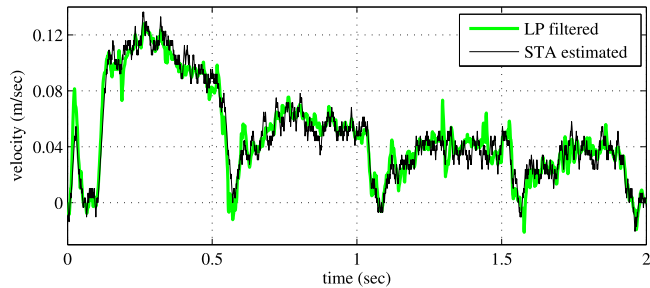


Fig. 3. STA estimated relative velocity versus low-pass (LP) filtered one taken as a reference measurement.

Section 4) obtained with the tuned STA-based exact robust differentiator (9) is exemplary shown in Fig. 3 over the low-pass (LP) filtered experimental relative velocity. Note that the experimental relative velocity is obtained via discrete-time differentiation of the measured relative displacement, and then assumed as the reference measurement upon LP-filtering. The details on designing the LP filter, with respect to the actuator time constants, are given below in Section 3.2.

3.2. Equivalent output injection

Next, consider the second-order system dynamics

$$\dot{x}_2 = g(u, x_2) + \xi(t) \quad (12)$$

perturbed by the unknown yet upper bounded $\xi(t) = m^{-1}F$, while an undisturbed system dynamics $g = m^{-1}(u - f(x_2))$ is assumed to be known, cf. with (1). For the perturbed case of the exact differentiator (8), (9), one introduces the state estimation error $\tilde{x}_2 = x_2 - \hat{x}_2$ which dynamics is governed by

$$\dot{\tilde{x}}_2 = g(u, x_2) + \xi(t) - k_2 \text{sign}(e). \quad (13)$$

The finite time convergence to the second-order sliding-mode set ensures that there exists a time constant $t_0 > 0$ such that for all $t \geq t_0$ the following identity holds (Davila et al., 2006)

$$0 \equiv \tilde{x}_2 \equiv g(u, x_2) + \xi(t) - k_2 \text{sign}(e). \quad (14)$$

Thereupon, an equivalent output injection, cf. Davila et al. (2006),

$$\chi \equiv k_2 \text{sign}(e) \equiv g(u, x_2) + \xi(t) \quad (15)$$

includes both, the known part of the system dynamics and the perturbation which estimation is of primary interest here. Since the equivalent output injection contains high-frequency discontinuous oscillations, due to the gained sign of the output error, a linear filtering process $G(\lambda)$ is inevitable. The unity gain low-pass transfer function G , with Laplace variable λ , can be arbitrarily designed, while taking into account chattering of the sliding-mode, as addressed below, and the bandwidth of

ξ . The latter is assumed to be approximately known in applications. Following to that, an equivalent output injection takes the form

$$\bar{\chi} = G(\lambda)[k_2 \text{sign}(e)], \quad (16)$$

while the low-pass filtered estimate of the second-order-dynamics perturbation results in

$$\hat{\xi}(t) = \bar{\chi}(t) - g(u(t), \hat{x}_2(t)). \quad (17)$$

Note that since the measured relative velocity is unavailable, the STA-based value is used in (17) for computing the unperturbed motion dynamics.

In order to rate the basic frequency ω_c of harmonic oscillations, i.e. chattering, one can use the harmonic balance analysis, which analytic solution is an estimate of the chattering parameters, i.e. amplitude and frequency (Ventura & Fridman, 2016, 2019). Assuming a nominal second-order actuator dynamics, with the time constant μ resulting in $\bar{u} = (\mu\lambda + 1)^{-2}u$, the harmonic oscillation frequency can be obtained as

$$\omega_c = \frac{K_\omega}{\mu} \quad \text{with} \quad K_\omega = \left(\frac{(1.748k_1)^2}{(1.748k_1)^2 + 4\pi k_2} \right)^{1/2}, \quad (18)$$

cf. Pérez-Ventura and Fridman (2019). The actuator time constant μ is assumed to be known or computable, as shown below for the recent case.

Taking into account the system dynamics (1), the actuator time constants relate to the phase lag of the closed-loop-controlled servo valve equally as to the dynamics of hydraulic circuits — prior to building up the actuating pressure in the cylinder chambers. The actuator time constant is assumed as the maximum

$$\mu = \max(\mu_v, \mu_h) \quad (19)$$

of both time constants, which are correspondingly associated: μ_v with the closed-loop-controlled servo valve and μ_h with hydraulic circuits of the actuated cylinder. While both can be directly computed

$$\mu_{v/h} = (\zeta_{v/h} \cdot \omega_{0,v/h})^{-1}, \quad (20)$$

from the associated damping factor ζ and eigenfrequency ω_0 , the latter should be determined or, at least, approximated separately. The eigenfrequency and damping parameters $\omega_{0,v} = 125.7$ rad/s and $\zeta_v = 0.8$ of the controlled servo-valve are determined from the measured frequency response function, see Pasolli and Ruderman (2018). For the hydraulic circuit, the parameters are obtained via a linearized hydraulic circuit modeling (Ruderman, 2017a), for which

$$\omega_{0,h} = 2A \sqrt{\frac{\beta}{\Omega m}} = 5873 \text{ rad/s}, \quad (21)$$

$$\zeta_h = \frac{\sigma}{4A} \sqrt{\frac{\Omega}{\beta m}} = 0.5. \quad (22)$$

Here Ω is the total volume in the hydraulic circuit and β is the bulk modulus. For more detail an interested reader is referred to Pasolli and Ruderman (2018) and Ruderman (2017a).

For approximately estimated chattering frequency $\omega_c = 71.1$ rad/s, the filtering process should be designed with cut-off frequency in a neighborhood to ω_c . A final tuning of the filter parameters is performed so that to minimize the equivalent output injection error with respect to the reference measurement of F . The low-pass filter transfer function, determined by the Butterworth filter design and transformed back into Laplace domain, results in

$$G(\lambda) = \frac{0.002\lambda^2 + 4.28\lambda + 8775}{\lambda^2 + 132.4\lambda + 8775}. \quad (23)$$

4. Higher-order sliding-mode based force estimation

The higher-order sliding-mode (HOSM) differentiator, proposed by Levant (2003), and since there further analyzed in multiple works, e.g. Cruz-Zavala and Moreno (2018) and Reichhartinger and Spurgeon (2018) to mention some of them here, allows for robust estimation of

the $(n - 1)$ th time derivative of the given signal $x_1(t)$. For designing a HOSM differentiator, the Lipschitz constant $L > 0$ of the highest (i.e. n th) time derivative of the (measured) input signal is assumed to be known, i.e. $|d^n x_1/dt^n| \leq L$. The HOSM differentiator of the $(n - 1)$ th order can be written in a generalized form

$$\dot{\hat{x}}_i = -k_i L^{\frac{i}{n}} |\hat{x}_1 - x_1|^{\frac{n-i}{n}} \text{sign}(\hat{x}_1 - x_1) + x_{i+1} \quad (24)$$

$$\dot{\hat{x}}_n = -k_n L \text{sign}(\hat{x}_1 - x_1), \quad (25)$$

cf. with Cruz-Zavala and Moreno (2018), for $i = 1, \dots, n - 1$. While the correspondingly powered L appears in the HOSM differentiator as a scaling factor, an optimal k_i -gains assignment remains continuously in focus of the ongoing research. In the following, an optimal parametric sets k_i is used, that is described in Reichhartinger et al. (2017) and based on a pseudo-linear representation of HOSM (Reichhartinger & Spurgeon, 2018). For that, the eigenvalues of characteristic polynomial with the differentiator gains are purposefully assignable.

Since the system exhibits the second-order dynamics, cf. (1), (12), a differentiator of the minimum second-order is required for estimating acceleration of the relative motion and thereupon predicting an external load force. Since the estimation accuracy of the i th derivative increases with increasing of the HOSM-order and, correspondingly, reduces with an increasing sampling time, see e.g. Livne and Levant (2014), the third-order HOSM differentiator is assumed in the following. While artificially increasing the order of HOSM differentiator, one solely requires an additional numerical integrator to be implemented and the higher-order Lipschitz constant to be determined. Here it is noted that a similar increase of the HOSM order has been equally justified for another system of hydraulic cylinders in Koch and Reichhartinger (2016). For the introduced output measurement error, cf. Section 3.1, the third-order HOSM differentiator (24), (25) results in

$$\begin{aligned} \dot{\hat{x}}_1 &= k_1 L^{\frac{1}{4}} |e|^{\frac{3}{4}} \text{sign}(e) + \hat{x}_2, \\ \dot{\hat{x}}_2 &= k_2 L^{\frac{1}{4}} |e|^{\frac{1}{2}} \text{sign}(e) + \hat{x}_3, \\ \dot{\hat{x}}_3 &= k_3 L^{\frac{3}{4}} |e|^{\frac{1}{4}} \text{sign}(e) + \hat{x}_4, \\ \dot{\hat{x}}_4 &= k_4 L \text{sign}(e). \end{aligned} \quad (26)$$

Recall that the same output error e , as for the STA-based estimation, is used while the Lipschitz constant L is inherently different here due to the fourth derivative of the HOSM differentiator, cf. with Section 3.1. An optimal gain setting

$$k_1, \dots, k_4 = \{4.1, 6.3, 4.3, 1.1\}, \quad (27)$$

proposed in Reichhartinger et al. (2017) is used, which is based on an approach described in detail in Reichhartinger and Spurgeon (2018).

The Lipschitz constant L , which is the single design parameter unknown in the system modeling, has been determined via a numerical optimization, based on the recorded experimental data, similar as in the case of STA. Solving numerically a minimization problem

$$\min_L \sum_{i=1}^N (\ddot{x}_i - \hat{\ddot{x}}_{3,i}(L))^2 \quad (28)$$

of the estimation error results in a locally optimal $L = 1040$. The size of the used experimental data set is denoted by N , while $\hat{\ddot{x}}_{3,i}$ is the estimated acceleration state in dependency of the varying L . The cumulative squared error is shown in Fig. 4 against the varying L , out of which an optimal gain setting is determined. Note that the differential order of the estimated state used for L -optimization is increased, comparing to the tuning of STA. Further recall that the goal here, differing from the case of STA-based cascade, is to obtain the acceleration quantity which is required for predicting the external load force with help of HOSM-based approach. Since the acceleration signal, obtained via double differentiation following by the LP-filtering, cf. with Section 3.1, is larger corrupted by the measurement and process noise, the determined optimization front is less smooth comparing to

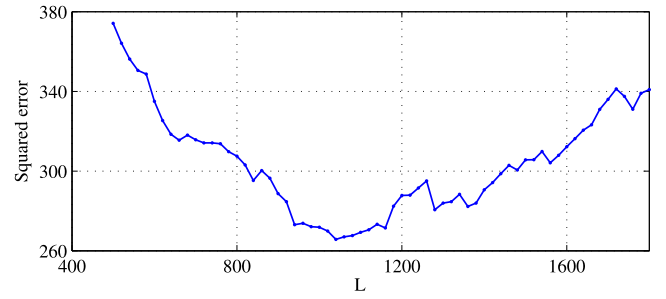


Fig. 4. Cumulative squared error $\sum(\ddot{x} - \hat{\ddot{x}}_3)^2$ against L , computed for determining the optimal HOSM-gains according to (26), (27).

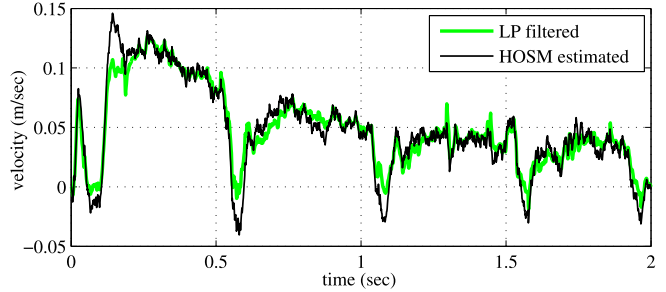


Fig. 5. HOSM estimated relative velocity versus low-pass (LP) filtered one taken as a reference measurement.

the STA tuning, cf. Figs. 2 and 4. Nevertheless, a local L -minimum is directly determinable from the obtained optimization front.

Since the HOSM-based algorithm provides equally an estimate of the relative velocity, used for computing $f(\cdot)$, the latter is compared with the reference value obtained via the discrete-time differentiation and LP-filtering of the encoder signal. The HOSM-estimated relative velocity is shown in Fig. 5 versus the reference measurement, cf. with STA-based estimation from Fig. 3. Both velocity estimates reveal sufficient similarity, while an absolute accuracy cannot be assessed due to unavailable exact measurement of the reference velocity.

Upon the HOSM-estimated relative velocity and acceleration of actuator motion, an external load force, correspondingly dynamics perturbation ξ , can be directly obtained for the second-order system (12). Note that in order to cope with the residual high-frequency components of signals in use, and to provide the same phase characteristics as before in the second-order SM approach, the computed dynamics perturbation is subject to the same low-pass filtering, cf. Section 3.2, thus resulting in

$$\hat{\xi} = G(\lambda)[\hat{x}_3 - g(u, \hat{x}_2)]. \quad (29)$$

5. Experimental evaluation

The experimental evaluation is made for the open-loop controlled drive of the right-hand side cylinder. A periodic counteracting force, produced by the left-hand side cylinder and recorded with the load-cell, has been applied, cf. Section 2.1. Two different load shapes have been generated, resulting in two motion profiles, shown in Fig. 6, and that of different frequencies and with varying amplitudes of the force. The corresponding input values of the measured pressure in both chambers are shown in Fig. 7. From both recorded position profiles one can notice a relatively high level of the sensor and (eventually) process noise when measuring $x(t)$.

The first motion profile is with sinusoidal counteraction at 0.4 Hz, that results in a trapezoidal-shaped load force the transient oscillations, cf. Fig. 8(a). The second one is with saw-shaped counteraction at 2 Hz, cf. Fig. 8 (b). During such (more steady) motion, the load force shows

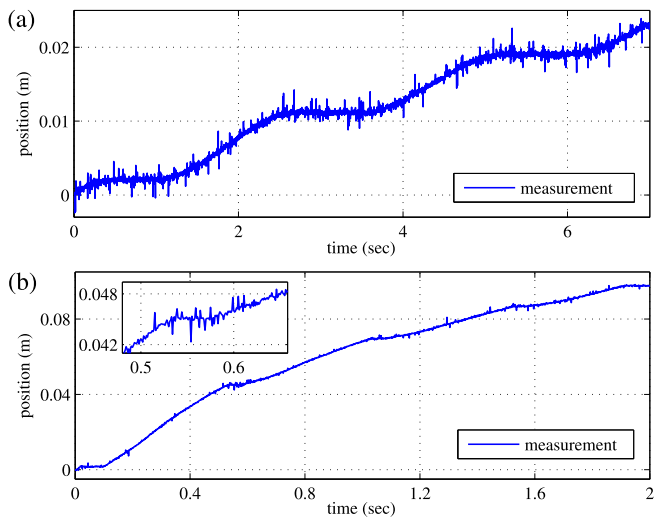


Fig. 6. Measured position from experiments with 0.4 Hz sinusoidal counteraction in (a) and 2 Hz saw-shaped counteraction in (b).

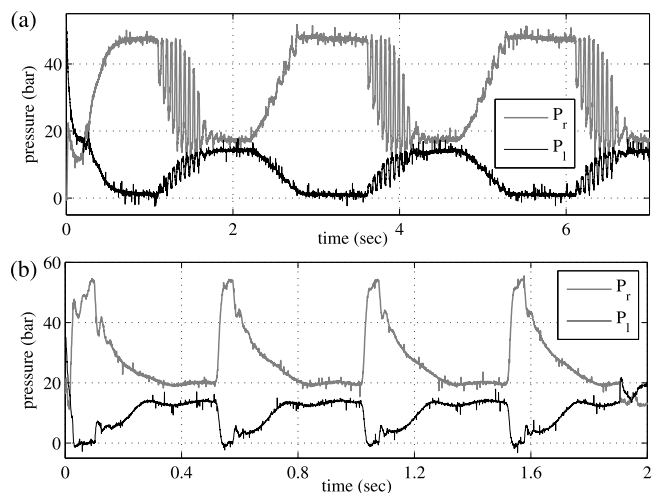


Fig. 7. Measured chambers pressure with 0.4 Hz sinusoidal counteraction in (a) and 2 Hz saw-shaped counteraction in (b).

a series of steeply peaks, followed by a flattening decrease of the magnitude. Note that both motion profiles have return to zero and zero crossing velocities, cf. Figs. 3 and 5, that strongly affects the dynamic friction and its model-based prediction.

Both, the second- and fourth-order sliding mode approaches, cf. Sections 3 and 4, have been real-time implemented and executed on the SpeedGoat platform, with the sampling rate set to 2 kHz, cf. Section 2.1. The used discrete-time integrators are the first-order forward Euler. The fixed-step discrete state solver of the Simulink Real-Time™ is used. The available and identified system parameters, with units, are provided in Table 1.

Experimental evaluation of the SM-based estimation of the counteracting load force are shown in Figs. 8, 9, and that for both motion profiles in (a) and (b) correspondingly. One can recognize that the oscillatory phases, equally as constant levels, of the load force are accurately reconstructed by the virtual sensing with the second- and fourth-order sliding modes techniques. Recall that the second-order sliding mode corresponds to the first-order differentiator and the fourth-order sliding mode corresponds to the third-order differentiator, cf. Section 4. The force estimation error depicted in Fig. 9 discloses that the performance

Table 1
System parameters.

Parameter	m	A	n	F_c	F_s	V
Units	kg	m ²	–	N	N	s/m
Value	1.7	0.0013	0.585	135	360	0.006
Parameter	δ	s	σ	α	τ	–
Units	–	–	N s/m	–	–	–
Value	1.5	150	350	3	0.005	–

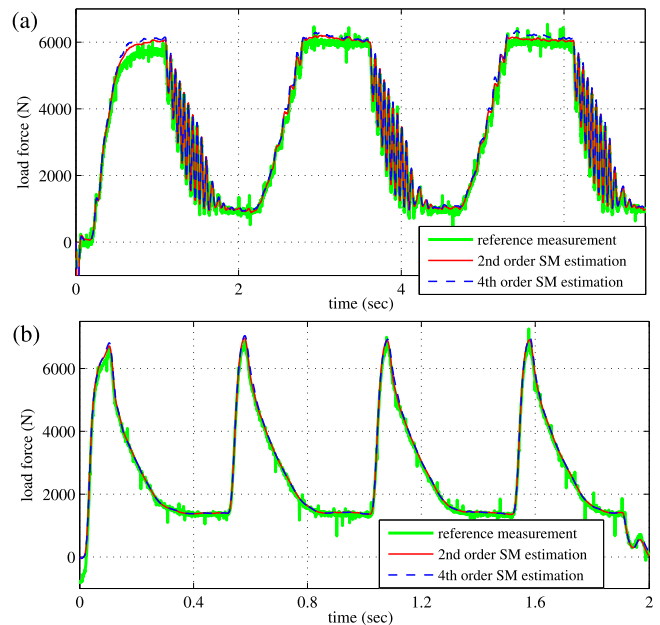


Fig. 8. Experimental evaluation of SM estimated load force. Measurement versus force prediction for 0.4 Hz sinusoidal counteraction in (a) and 2 Hz saw-shaped counteraction in (b).

of both approaches is well comparable, while the HOSM-based estimation exhibits a slightly higher peaking at zero crossing velocity. This can be explained by differing velocity estimates with the STA- and HOSM-based differentiators, which reflects in computing of $f(\cdot)$, correspondingly $g(\cdot)$ and directly affects the accuracy of $\hat{\xi}$ -estimate. Further it can be noted that both the STA- and HOSM-based estimation of the load force suffer under similar negative bias of about 200 N. The latter lies, however, in the range of some 3% of the maximal applied external force, and can be associated either with a bias of the load-cell sensor or with modeling bias in the $g(\cdot)$ mapping. One can stress that for the generally known challenges and inaccuracies associated with force measurements, the force estimation errors (Fig. 9) including bias are tolerable for the given range of load variations.

6. Conclusions

For the external load forces, generally unknown in the controlled hydraulic actuators, a virtual sensing approach based on the second- and higher-order sliding modes has been proposed. Measuring the noisy relative displacement, i.e. cylinder stroke, and the pressure-difference-based driving hydraulic force, the relative velocity of cylinder piston is estimated by means of the exact differentiator with an optimal gains setting. Based thereupon, an equivalent output injection of the second-order sliding-mode has been used for perturbation force estimation, correspondingly ‘virtual sensing’. For the sake of comparison, the fourth-order differentiator has been used based on the HOSM techniques, out of which the velocity and acceleration estimates are obtained. For both SM-based strategies the same second-order system behavior, including nonlinear dynamic friction, has been assumed

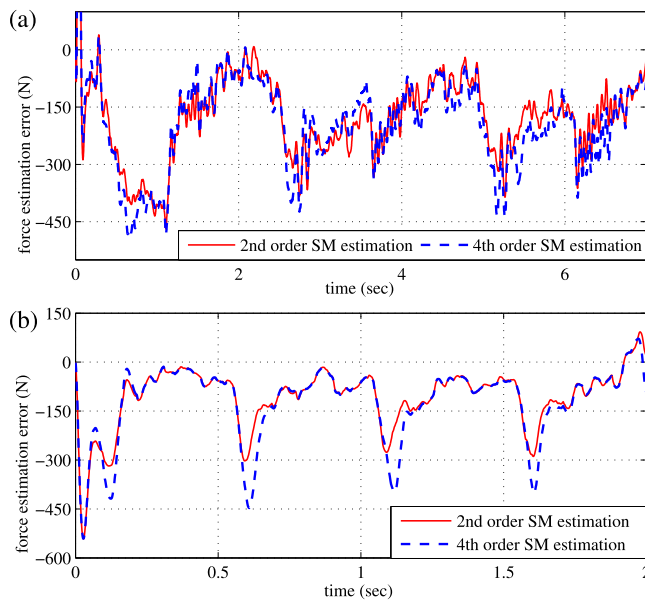


Fig. 9. Force estimation error for 0.4 Hz sinusoidal counteraction in (a) and 2 Hz saw-shaped counteraction in (b).

while the lumped moving mass and friction parameters are identified as nominal before applying the external load forces. A robust reconstruction of the varying load forces and that for different – step-like transient, oscillatory, and constant – conditions has been demonstrated. The evaluation results are shown on the experimental data which has considerable level of the process and measurement noise.

Declaration of competing interest

None declared.

Acknowledgments

This work has received funding from the European Union Horizon 2020 research and innovation programme H2020-MSCA-RISE-2016 under the grant agreement No 734832. Second author also acknowledges support from Consejo Nacional de Ciencia y Tecnología (CONACYT), Mexico, grant no. 282013 and Programa de Apoyo a Proyectos de Investigación e Innovación Tecnológica (PAPIIT-UNAM), Mexico, grant no. IN 115419.

References

- Al-Bender, F., & Swevers, J. (2008). Characterization of friction force dynamics. *IEEE Control Systems Magazine*, 28(6), 64–81.
- Alleyne, A., & Liu, R. (2000). A simplified approach to force control for electro-hydraulic systems. *Control Engineering Practice*, 8(12), 1347–1356.
- Armstrong, B., Dupont, P., & De Wit, C. C. (1994). A survey of modeling, analysis tools and compensation methods for the control of machines with friction. *Automatica*, 30, 1083–1138.
- Bonchis, A., Corke, P. L., Rye, D. C., & Ha, Q. P. (2001). Variable structure methods in hydraulic servo systems control. *Automatica*, 37(4), 589–595.
- Cruz-Zavala, E., & Moreno, J. A. (2018). Levant's arbitrary order exact differentiator: A Lyapunov approach. *IEEE Transactions on Automatic Control*, 64(7), 3034–3039.
- Dahl, P. R. (1968). A solid friction model, TOR 158(3107-18), The Aerospace Corporation, El Segundo.
- Davila, J., Fridman, L., & Poznyak, A. (2006). Observation and identification of mechanical systems via second order sliding modes. *International Journal of Control*, 79(10), 1251–1262.
- Ha, Q., Nguyen, Q., Rye, D., & Durrant-Whyte, H. (2000). Impedance control of a hydraulically actuated robotic excavator. *Automation in Construction*, 9(5–6), 421–435.
- Haga, M., Hiroshi, W., & Fujishima, K. (2001). Digging control system for hydraulic excavator. *Mechatronics*, 11(6), 665–676.

- Jelali, M., & Kroll, A. (2012). *Hydraulic servo-systems: modelling, identification and control*. Springer.
- Jerouane, M., Sepehri, N., & Lamnabhi-Lagarrigue, F. (2004). Dynamic analysis of variable structure force control of hydraulic actuators via the reaching law approach. *International Journal of Control*, 77(14), 1260–1268.
- Koch, S., & Reichhartinger, M. (2016). Observer-based sliding mode control of hydraulic cylinders in the presence of unknown load forces. *Elektrotechnik und Informationstechnik*, 133, 253–260.
- Koizumi, T., & Shibazaki, H. (1984). A study of the relationships governing starting rolling friction. *Wear*, 93(3), 281–290.
- Komsta, J., van Oijen, N., & Antoszkiewicz, P. (2013). Integral sliding mode compensator for load pressure control of die-cushion cylinder drive. *Control Engineering Practice*, 21(5), 708–718.
- Küchler, S., Mahl, T., Neupert, J., Schneider, K., & Sawodny, O. (2011). Active control for an offshore crane using prediction of the vessels motion. *IEEE/ASME Transactions on Mechatronics*, 16(2), 297–309.
- Lawrence, P. D., Salcudean, S. E., Sepehri, N., Chan, D., Bachmann, S., Parker, N., et al. (1997). Coordinated and force-feedback control of hydraulic excavators. In *Experimental robotics IV* (pp. 181–194).
- Levant, A. (1993). Sliding order and sliding accuracy in sliding mode control. *International Journal of Control*, 58(6), 1247–1263.
- Levant, A. (1998). Robust exact differentiation via sliding mode technique. *Automatica*, 34(3), 379–384.
- Levant, A. (2003). Higher-order sliding modes, differentiation and output-feedback control. *International Journal of Control*, 76(9–10), 924–941.
- Livne, M., & Levant, A. (2014). Proper discretization of homogeneous differentiators. *Automatica*, 50(8), 2007–2014.
- Loukianov, A. G., Rivera, J., Orlov, Y. V., & Teraoka, E. Y. M. (2009). Robust trajectory tracking for an electrohydraulic actuator. *IEEE Transactions on Industrial Electronics*, 56(9), 3523–3531.
- Marques, F., Flores, P., Claro, J. P., & Lankarani, H. M. (2016). A survey and comparison of several friction force models for dynamic analysis of multibody mechanical systems. *Nonlinear Dynamics*, 86(3), 1407–1443.
- Mattila, J., Koivumäki, J., Caldwell, D. G., & Semini, C. (2017). A survey on control of hydraulic robotic manipulators with projection to future trends. *IEEE/ASME Transactions on Mechatronics*, 22(2), 669–680.
- Merritt, H. E. (1967). *Hydraulic control systems*. John Wiley & Sons.
- Ortiz Morales, D., Westerberg, S., La Hera, P. X., Mettin, U., Freidovich, L., & Shiriaev, A. S. (2014). Increasing the level of automation in the forestry logging process with crane trajectory planning and control. *Journal of Field Robotics*, 31(3), 343–363.
- Osakada, K., Mori, K., Altan, T., & Groche, P. (2011). Mechanical servo press technology for metal forming. *CIRP Annals-Manufacturing Technology*, 60(2), 651–672.
- Pasolli, P., & Ruderman, M. (2018). Linearized piecewise affine in control and states hydraulic system: modeling and identification. In *IEEE 44th annual conference of the industrial electronics society (IECON)* (pp. 4537–4544).
- Pasolli, P., & Ruderman, M. (2019). Hybrid state feedback position-force control of hydraulic cylinder. In *IEEE international conference on mechatronics (ICM)* (pp. 54–59).
- Pedersen, H. C., & Andersen, T. O. (2018). Pressure feedback in fluid power system-active damping explained and exemplified. *IEEE Transactions on Control Systems Technology*, 26(1), 102–113.
- Pérez-Ventura, U., & Fridman, L. (2019). When is it reasonable to implement the discontinuous sliding-mode controllers instead of the continuous ones? frequency domain criteria. *International Journal of Robust and Nonlinear Control*, 29(3), 810–828.
- Plummer, A. R., & Vaughan, N. (1996). Robust adaptive control for hydraulic servosystems. *Journal of Dynamic Systems, Measurement, and Control*, 118(2), 237–244.
- Reichhartinger, M., & Spurgeon, S. (2018). An arbitrary-order differentiator design paradigm with adaptive gains. *International Journal of Control*, 91(9), 1–15.
- Reichhartinger, M., Spurgeon, S., Forstinger, M., & Wipfler, M. (2017). A robust exact differentiator toolbox for matlab®/simulink®. *IFAC-PapersOnLine*, 50(1), 1711–1716.
- Rokseth, B., Skjong, S., & Pedersen, E. (2016). Modeling of generic offshore vessel in crane operations with focus on strong rigid body connections. *IEEE Journal of Oceanic Engineering*, 42(4), 846–868.
- Ruderman, M. (2017a). Full-and reduced-order model of hydraulic cylinder for motion control. In *IEEE 43th annual conference of the industrial electronics society (IECON)* (pp. 7275–7280).
- Ruderman, M. (2017b). On break-away forces in actuated motion systems with nonlinear friction. *Mechatronics*, 44, 1–5.
- Ruderman, M., & Bertram, T. (2011). Modified maxwell-slip model of presliding friction, In *Proc. 18th IFAC world congress (2011)*, (pp. 10764–10769).
- Ruderman, M., & Fridman, L. (2018). Use of second-order sliding mode observer for low-accuracy sensing in hydraulic machines. In *IEEE 15th international workshop on variable structure systems (VSS)* (pp. 315–318).
- Ruderman, M., & Iwasaki, M. (2015). Observer of nonlinear friction dynamics for motion control. *IEEE Transactions on Industrial Electronics*, 62(9), 5941–5949.
- Ruderman, M., & Iwasaki, M. (2016). Analysis of linear feedback position control in presence of presliding friction. *IEEE Journal of Industry Applications*, 5(2), 61–68.

- Ruderman, M., & Rachinskii, D. (2017). Use of Prandtl-Ishlinskii hysteresis operators for coulomb friction modeling with presliding. *Journal of Physics: Conference Series*, 811(1), 012013.
- Shtessel, Y., Edwards, C., Fridman, L., & Levant, A. (2014). *Sliding mode control and observation*. Springer.
- Striebeck, R. (1902). Die wesentlichen eigenschaften der gleit- und rollenlager. *VDI-Zeitschrift (in German)*, 46(36–38), 1341–1348,1432–1438,1463–1470.
- Taylor, C., & Robertson, D. (2013). State-dependent control of a hydraulically actuated nuclear decommissioning robot. *Control Engineering Practice*, 21(12), 1716–1725.
- Utkin, V., Guldner, J., & Shi, J. (2009). *Sliding mode control in electro-mechanical systems*. CRC press.
- Vázquez, C., Aranovskiy, S., Freidovich, L. B., & Fridman, L. M. (2016). Time-varying gain differentiator: A mobile hydraulic system case study. *IEEE Transactions on Control Systems Technology*, 24(5), 1740–1750.
- Ventura, U. P., & Fridman, L. (2016). Chattering measurement in SMC and HOSMC. In *IEEE 14th international workshop on variable structure systems (VSS)* (pp. 108–113).
- Ventura, U. P., & Fridman, L. (2019). Design of super-twisting control gains: a describing function based methodology. *Automatica*, 99, 175–180.
- Won, D., Kim, W., & Tomizuka, M. (2017). High-gain-observer-based integral sliding mode control for position tracking of electrohydraulic servo systems. *IEEE/ASME Transactions on Mechatronics*, 22(6), 2695–2704.
- Yao, B., Bu, F., Reedy, J., & Chiu, G.-C. (2000). Adaptive robust motion control of single-rod hydraulic actuators: theory and experiments. *IEEE/ASME Transactions on Mechatronics*, 5(1), 79–91.